photonics

MDPI

Article

Determination of Main Spectral and Luminescent Characteristics of Winter Wheat Seeds Infected with Pathogenic Microflora

Alexey M. Bashilov [1], Igor Yu. Efremenkov [2], Mikhail V. Belyakov [3], Alexander V. Lavrov [3], Anatoly A. Gulyaev [3,*], Stanislav A. Gerasimenko [3], Sergei I. Borzenko [3] and Andrey A. Boyko [4]

[1] Moscow Aviation Institute, National Research University, Volokolamsk Highway, 4, 125993 Moscow, Russia; bashilov@inbox.ru
[2] Branch of Moscow Energy Institute, National Research University, Energy Passage 1, 214013 Smolensk, Russia; efremenkovigor55@mail.ru
[3] Federal Scientific Agroengineering Center VIM, 1st Institutsky Proezd 5, 109428 Moscow, Russia; bmw20100@mail.ru (M.V.B.); vimlavrov@mail.ru (A.V.L.); stanislav.mkm@gmail.com (S.A.G.); Borzencko.serzh@yandex.ru (S.I.B.)
[4] Don State Technical University, Gagarin Square, 1, 344000 Rostov-on-Don, Russia; andreyboi@yandex.ru
* Correspondence: tomasss1086@mail.ru; Tel.: +7-918-501-44-74

Abstract: In connection with the constant growth of demand for high-quality food products, there is a need to develop effective methods for storing agricultural products, and the registration and predicting infection in the early stages. The studying of the physical properties of infected plants and seeds has fundamental importance for determining crop losses, conducting a survey of diseases, and assessing the effectiveness of their control (assessment of the resistance of crops and varieties, the effect of fungicides, etc.). Presently, photoluminescent methods for diagnosing seeds in the ultraviolet and visible ranges have not been studied. For research, seeds of winter wheat were selected, and were infected with one of the most common and dangerous diseases for plants—fusarium. The research of luminescence was carried out based on a hardware–software complex consisting of a multifunctional spectrofluorometer "Fluorat-02-Panorama", a computer with software "Panorama Pro" installed, and an external camera for the samples under study. Spectra were obtained with a diagnostic range of winter wheat seeds of 220–400 nm. Based on the results obtained for winter wheat seeds, it is possible to further develop a method for determining the degree of fusarium infection.

Keywords: winter wheat seeds; fusarium; photoluminescence; spectrum; Gaussians

Citation: Bashilov, A.M.; Efremenkov, I.Y.; Belyakov, M.V.; Lavrov, A.V.; Gulyaev, A.A.; Gerasimenko, S.A.; Borzenko, S.I.; Boyko, A.A. Determination of Main Spectral and Luminescent Characteristics of Winter Wheat Seeds Infected with Pathogenic Microflora. *Photonics* **2021**, *8*, 494. https://doi.org/10.3390/photonics8110494

Received: 27 September 2021
Accepted: 2 November 2021
Published: 4 November 2021

1. Introduction

The constant increase in the need for high-quality food products, their efficient production, and storage in sterile conditions is caused not only by the growth of population, but also by the emergence of new diseases affecting huge stocks of food products. In this regard, technologies for storing agricultural products and registering and predicting infection are needed at early stages. The study of the physical properties of infected plants and seeds is of fundamental importance for determining crop losses, conducting a disease survey, setting thresholds when making decisions, obtaining new knowledge about the epidemiology of diseases, and evaluating the effectiveness of combating them (assessing the resistance of crops and varieties, the effect of fungicides, etc.).

The first methods of determining the degree of infection are visual, but they are subjective, and they show themselves to be ineffective and inaccurate at the early stages of infection. The diagnosis is carried out manually, analyzing such indicators as the shape of grain, the characteristics of its surface (surface color and gloss), the structure of the endosperm (vitreous, consistency), the color of the embryo, etc.

Laboratory methods do not have such disadvantages. They have a fairly high accuracy and reproducibility, but large time and economic costs also do not make them optimal for predicting food contamination. Mycological analysis, enzyme immunoassay, real-time PCR [1,2], and quantitative digital PCR, using markers based on intergenic spacers [3], are used to diagnose fusarium lesions. The common disadvantages of these methods are extremely expensive equipment and reagents, the duration of the analysis of up to 7–10 days, and the need for highly qualified specialists to conduct them.

Technologies that can replace or complement visual assessments are sensor-based image analysis, including visible spectrum sensors, and hyperspectral (HSI) and multispectral (MSI) sensors [4–10]. These technologies make it possible to accurately measure the severity of the disease in controlled conditions, but have not yet demonstrated their full potential for accurate measurement in field conditions. Sensor technology is developing rapidly, and artificial intelligence can help overcome problems with measurement automation [11,12].

Unlike RGB cameras, which have a spatial resolution of several megapixels, spectral sensors have a higher resolution [13]. HSI and MSI sensors evaluate narrow wave ranges combined with high spatial resolution. The visible and near-infrared regions have the greatest amount of information for monitoring plant stress. The ultraviolet range [14] and the SWIR range [15] also provide information. Spectral sensors can be characterized by the resolution and the type of a detector. Often, MSI sensors cover the visible and near-infrared range, but provide less data due to lower spectral resolution, although they are lightweight and cheaper [13]. On the contrary, HSI sensors are more complex, heavy, expensive, and measurements take longer and require strict protocols. The systems consist of a sensor, a light source, and a control unit for measuring, storing, and processing data [16].

There are also other sensory methods for quantifying diseases or pathogens (thermal imaging, chlorophyll fluorescence).

To date, photoluminescent diagnostic methods in the ultraviolet and visible ranges have not been studied. They, as with other optical methods, are highly accurate, selective, expressive, as well as distant and non-destructive; moreover, they have lower economic costs compared to previous methods. Their other advantages are the simplicity and safety of operation of devices for their implementation, a minimum of subjective factors and the possibility of integration into existing modern agricultural machines and units.

Chlorophyll fluorescence is a promising method for research the quality of fruit after harvest. The HSI method was used to measure the laser-induced fluorescence of apple fruit to predict several parameters of fruit quality [17]. Reducing the chlorophyll content in plant leaves is a means of early diagnosis of plant diseases. The occurrence of diseases affects the fluorescence of phenolic compounds and chlorophyll in grapefruit fruit [18] and other citrus fruit [19]. The fluorescence spectra of the surface parts of healthy and infected apples and potatoes were studied [20]. Two zones were found for apples, where the radiation spectra of healthy samples and samples affected by scab differed significantly from each other. A similar zone was found for potato root crops. The revealed differences in fluorescence spectra can be used to detect and separate diseased and healthy fruit and vegetables. In our work, we search for spectral regions, characteristics, and parameters of excitation and luminescence spectra to determine winter wheat seeds infected with pathogenic *Fusarium* microflora.

2. Materials and Methods

One of the most common and dangerous diseases for plants, and no less dangerous for humans, is fusarium, the causative agents of which are fungi of the genus fusarium. Winter wheat seeds were used as biomaterial.

Obtaining the spectral characteristics of the luminescence of winter wheat seeds "Irishka No. 172". Pedigree: Ind. O. from a hybrid population created with the participation of a ligulless line of mutant origin 86 lg 333 and varieties Obriy, Skifianka. Included in the State Register for the North Caucasus (6) region. Recommended for cultivation in the North, West-delta, South-foothill zones of the Krasnodar Territory; in the Central zone of

the Stavropol Territory; Priazovskaya, southern and eastern zones of the Rostov region. A kind of lutescens. Colored caryopsis. The mass of 1000 grains is 34–45 g. The average yield in the region is 48.2 c/ha. In the Krasnodar Territory, black and busy steam, the increase to the Palpich standard was 3.9 c/ha, in the southern and eastern zones of the Rostov region to the standard Zernogradka 10–5.7 c/ha, in the Central, Mountain and Foothill zones of the Stavropol Territory. Row-crop predecessors to the average standard−3.5 c/ha had a yield of 58.7; 64.7 and 59.0 c/ha, respectively. Valuable wheat: According to the applicant, highly resistant to storm and stem rust; moderately resistant to yellow rust, powdery mildew; moderately susceptible to septoria and fusarium spike; moderately susceptible to hard smut. Properties of the Irishka variety: Recommended region: North Caucasian. Direction of use: valuable in terms of quality Ripening period: medium early. This sample is the harvest of 2020, the Central Black Earth zone of Russia.

In the studied seed fractions, the degree of damage to *p. Fusarium* seeds was determined. The research was conducted at the Federal Center for Safety and Quality Assessment of Grain and Processed Products by the Federal Service for Veterinary and Phytosanitary Surveillance. Sample weight −3.2 kg. Definition of fusarium grains according to GOST 31646-2012 (RF) "Grain crops. Method for determining the content of fusarium grains". Equipment: liquid Prominence chromatograph with spectroscopic detector SPD-M20A, spectrofluorimetric detector RF-20AXS. The degree of seed damage was 98%.

The study of luminescence was carried out based on the hardware and software complex consisting of the multifunctional spectrofluorometer "Fluorat-02-Panorama", a computer with the software "Panorama Pro" installed and an external camera for the samples under study. During measurements, the intensity of the luminescence photosignal depends on the intensity of excitation. This is taken into account in the Panorama Pro program. Additionally, the photo signal depends on the exposure time (t = 1.5 microseconds) and the sensitivity of the photoelectric multiplier. These parameters, as well as the parameters of the radiation source, remain unchanged when measuring healthy and infected seeds. The measurement of the excitation and photoluminescence spectra was carried out similarly to the previously performed measurements [21].

The excitation specters η_e (λ) and on their basis, the luminescence specters φ_l (λ) were measured with synchronous scanning. Synchronous scanning involves simultaneous restructuring of the monochromators of the excitation channels and registration of luminescence at a fixed value of their displacement, preferably close to the Stokes shift. In this case, the maximum value of the signal is obtained. The statistical processing was carried out according to the measurement results, where averaging over 250 specters was carried out. In the PanoramaPro program, the integral parameters of the H and Φ spectra were calculated. The latter is the photoluminescence flux expressed in relative units (r. u.).

$$H = \int_{\lambda_1}^{\lambda_2} \eta_e(\lambda) d\lambda, \quad (1)$$

$\eta_e(\lambda)$ is the spectral characteristics of the excitation
$\lambda_1 \ldots \lambda_2$ are limits of the operating spectral range of excitation.

$$\Phi = \int_{\lambda_1}^{\lambda_2} \varphi_l(\lambda) d\lambda, \quad (2)$$

$\varphi_l(\lambda)$ is spectral characteristics of photoluminescence,
$\lambda_1 \ldots \lambda_2$ are limits of the operating spectral range of photoluminescence.

The photoluminescence spectrum is continuous, and it is continuous in the range of measured wavelengths. The mathematical expectation (mean value) M_λ is determined by the integral:

$$M_\lambda = \int_{\lambda_{min}}^{\lambda_{max}} \lambda \varphi(\lambda) d\lambda, \quad (3)$$

where $\varphi(\lambda)$ is differential distribution function (probability density distribution);

λ is wavelength, nm;

λ_{min}, λ_{max} are minimum and maximum value of wavelength range of photoluminescence measurements, nm.

Dispersion σ^2 is determined by the formula:

$$\sigma^2 = \int_{\lambda_{min}}^{\lambda_{max}} (\lambda - M_\lambda)^2 \varphi(\lambda)\, d\lambda. \quad (4)$$

The numerical characteristic of the asymmetry (skewness) is the central static moment of the 3rd order μ_3:

$$\mu_3 = \int_{\lambda_{min}}^{\lambda_{max}} (\lambda - M_\lambda)^3 \varphi(\lambda)\, d\lambda. \quad (5)$$

In practice, the asymmetry coefficient is used to evaluate the asymmetry *As*:

$$As = \frac{\mu_3}{\sigma^3}, \quad (6)$$

where σ is the standard deviation.

With right-sided asymmetry (the "tail" of the spectrum curve is stretched to the right) $As > 0$. With left-sided symmetry (the "tail" of the spectrum curve is stretched to the left) $As < 0$. The numerical characteristic of the steepness of the spectrum is the estimate of the central static moment of the 4th order μ_4:

$$\mu_4 = \int_{\lambda_{min}}^{\lambda_{max}} (\lambda - M_\lambda)^4 \varphi(\lambda)\, d\lambda. \quad (7)$$

In practice, an artificially created value is taken as an estimate of the steepness coefficient, which is called the kurtosis E_λ:

$$E_\lambda = \frac{\mu_4}{\sigma^4} - 3. \quad (8)$$

For curves that are steeper (more island-like) than the curve of the normal distribution (bell-shaped curve), the kurtosis is positive, and the kurtosis is negative for

The largest absolute value of the negative kurtosis is 2. At this value, the vertex of the curve falls to the kurtosis axis and the curve is divided into two independent peaks and their analysis should be considered separately. The positive value of the kurtosis can be any type.

To obtain the equation of the numerical characteristic of the photoluminescence energy, it should be taken into account that each photon of photoluminescence has an energy associated with the radiation wavelength by the ratio:

$$E_{ph} = \frac{1240}{\lambda}, \quad (9)$$

where E_{ph} is measured in eV, and λ—in nm. If the differential distribution function $\varphi(\lambda)$ is known, then the total energy of the spectrum in the wavelength range is as:

$$E = 1240 \int_{\lambda_{\min}}^{\lambda_{\max}} \frac{1}{\lambda} \varphi(\lambda)\, \mathrm{d}\lambda. \quad (10)$$

To select the optimal value of the monochromator displacement, the spectral characteristics of the excitation were measured during synchronous scanning of wheat seeds in the spectral range of 180–700 nm.

To implement this stage, 20 uninfected wheat seeds were selected, after which a synchronous scan of each seed was performed, followed by averaging the results.

The next stage of spectrum processing is their decomposition into elementary bands. One of the main problems of high-quality photoluminescence analysis is the separation of a wide experimental spectrum into elementary bands and the determination of the parameters of individual radiation bands. For this purpose, such methods of decomposition of experimental photoluminescence spectra into individual bands as the Alentsev–Fock method, λ-modulation, and derivative spectroscopy are mainly used. At the same time, each of the methods has its own limitations. The Alentsev–Fock method requires significant differences in photoluminescence spectra while maintaining the unchanged shape of individual bands in the spectra. The disadvantage of the λ-modulation method is its low noise immunity. In the method of derivative spectroscopy, the accuracy of determining the half-width of the spectrum and the order of the derivative is insufficient. Computer modeling is divorced from real physical processes, and it is difficult to associate the individual bands found with real photoluminescence centers.

A method is proposed for decomposing the sum of Gaussian functions that make up the experimental photoluminescence spectrum into individual bands. It is implemented based on simple mathematical operations. The method of decomposition of the sum of Gaussian functions has been tested on the example of solving the problem of identifying the parameters of individual bands in the photoluminescence spectrum. The parameters of individual bands are close to those obtained by the Alentsev–Fock and derivative spectroscopy methods [22].

The decomposition into Gaussians was carried out according to the method described in [23]. To obtain Gauss curves, the spectral characteristics of luminescence were smoothed, after which, to determine the differential distribution function of the spectrum, it is necessary to divide the ordinates of the luminescence spectrum curve by the numerical value of the area bounded by the curve, i.e., normalize the area, which will be the future axis of the ordinates. To create the abscissa axis, i.e., to transition from wavelengths to the frequency range, it is necessary to divide the coefficient 1240 (see Formula (9)) by the abscissa curve of the luminescence spectrum. After constructing the abscissa axis and the ordinate axis, using the hardware capabilities of the Microcal Origin program, multi-peak processing was carried out, i.e., direct decomposition of the luminescence spectral characteristic into Gaussian curves. The error of the decomposition into Gaussians is about 0.018%.

3. Results

Figure 1 shows the excitation spectra during synchronous scanning of wheat seeds in the spectral range of 180–700 nm with a displacement of monochromator excitation and registration from 50 to 100 nm.

When the displacement value changes, the spectral characteristics of the excitation differ from each other not only quantitatively, but also qualitatively: when the displacement of monochromators increases, the left part of the spectrum shifts to the left, and the right part practically does not change. Table 1 shows the integral parameters of the excitation spectra of wheat seeds, which were calculated using Formula (1).

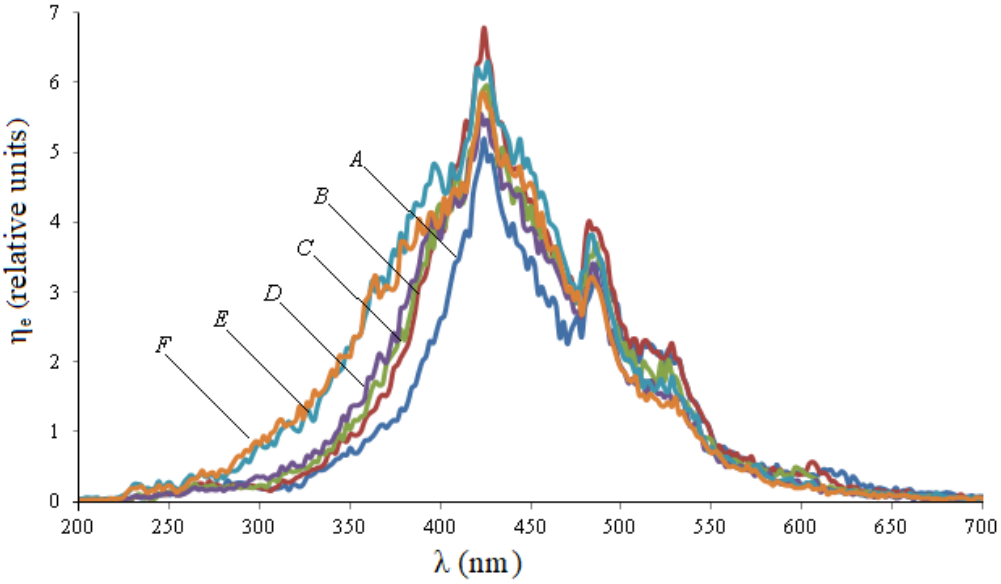

Figure 1. Excitation spectra η_e (λ) for synchronous scanning of wheat seeds at the displacement: A—50 nm, B—60 nm, C—70 nm, D—80 nm, E—90 nm, F—100 nm.

Table 1. Integral parameters of the excitation spectra of wheat seeds.

Displacement Value, nm	50	60	70	80	90	100
H, r. u.	583	719	685	662	816	761

It follows from Table 1 that when the displacement value is equal to 90 nm, the integral parameter of the absorption spectrum H is the maximum and is equal to 816 r.u., therefore we will use it for further measurements.

Knowing the optimal value of the displacement, 250 measurements were carried out with simultaneous scanning of infected and uninfected seeds. The average results of wheat seed measurements are shown in Figure 2.

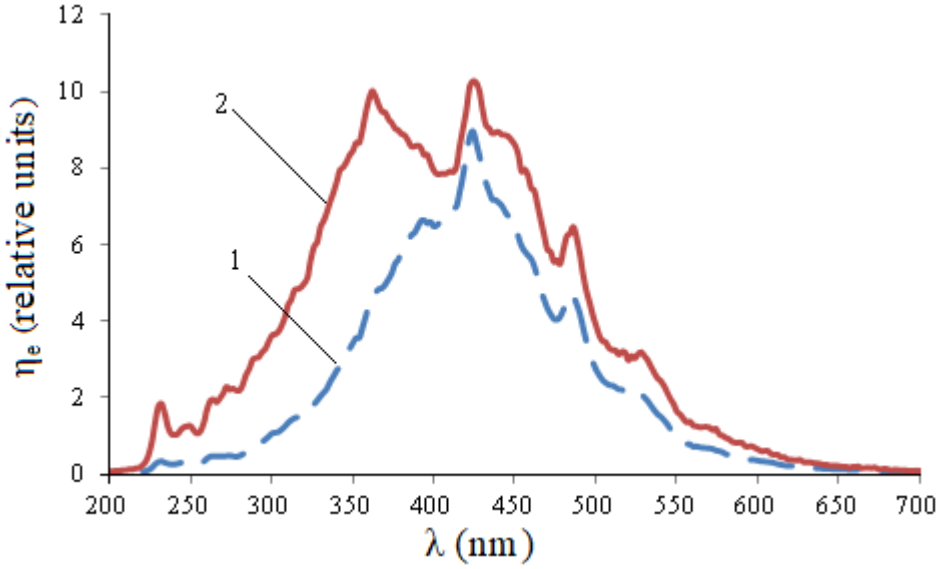

Figure 2. Spectral characteristics of excitation of wheat seeds during synchronous scanning: 1—not infected, 2—98% infected.

It follows from Figure 2 that during infection, wheat seeds have a maximum at a wavelength of 232 nm, and there is also a quantitative increase in peaks at wavelengths: 362 nm, 424 nm, 485 nm. The integral parameters of excitation spectra of wheat seeds of various degrees of fusarium infection in different spectral ranges corresponding to the maxima are presented in Table 2.

Table 2. Integral parameters of the excitation spectra of wheat seeds of various degrees of Fusarium infection.

Degree of Infection with Fusarium, %	H, r. u.	H, r. u. (for the Spectral Range, nm)				
		220–240	340–400	400–460	460–510	510–550
0	1135	4	296	426	194	72
98	1882	23	530	522	269	108

Thus, in infected seeds, the integral absorption capacity of H in the range of 220–240 nm (peak 232 nm) exceeds the same indicator for healthy seeds by 5.75 times, in the range of 340–400 nm (peak 362 nm) by 1.79 times. For other ranges, this ratio is lower: for 400–460 nm (peak 424 nm)—1.22 times, 460–510 nm (peak 485 nm)—1.39 times, 510–550 nm (peak 528 nm)—1.5 times.

Knowing from Figure 2 the wavelengths of the excitation maxima λe, we measure the photoluminescence spectra $\varphi_l(\lambda)$. To do this, the excitation channel monochromator is set to the wavelength λ_e, and the luminescence channel monochromator scans a longer wavelength range, registering the spectral flux density $\varphi_l(\lambda)$. Figures 3–7 show the spectral characteristics of luminescence averaged over 250 measurements at various λ_e.

It follows from Figure 3 that the luminescence spectrum lies in the range of approximately 290–374 nm. The integral parameter of the spectrum—the relative photoluminescence flux—in this range is determined by Formula (2).

The maximum values of spectral characteristics for infected and uninfected seeds differ by 2.58 times. Photoluminescence fluxes at $\lambda_{e,1}$ = 232 nm differ by 2.64 times. This confirms the significance of the spectral differences of $\eta_e(\lambda)$ in the range 220–240 nm in Figure 2. At the same time, the photo signal is relatively small.

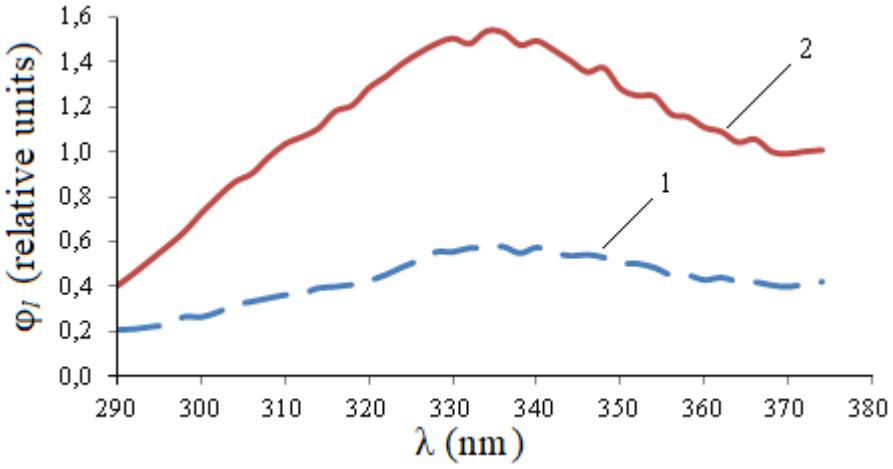

Figure 3. Spectral characteristics of luminescence of wheat seeds at $\lambda_{e,1}$ = 232 nm: 1—not infected, 2—98% infected.

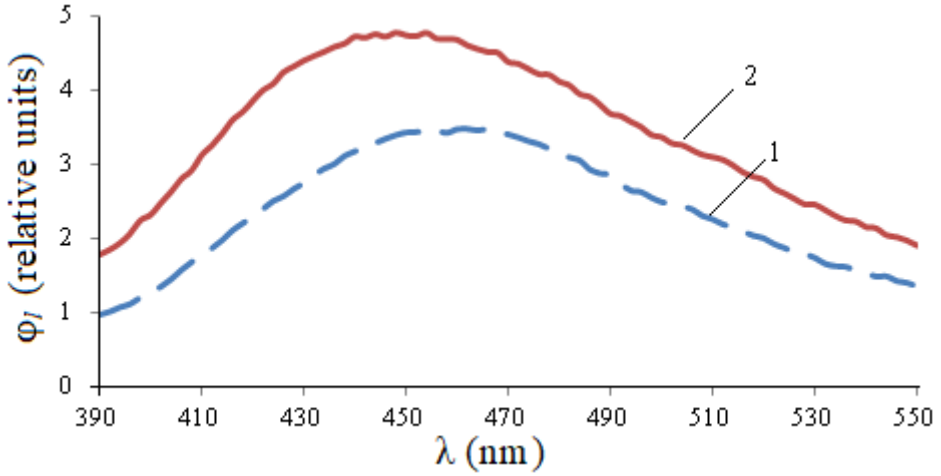

Figure 4. Spectral characteristics of luminescence of wheat seeds at $\lambda_{e,2}$ = 362 nm: 1—not infected, 2—98% infected.

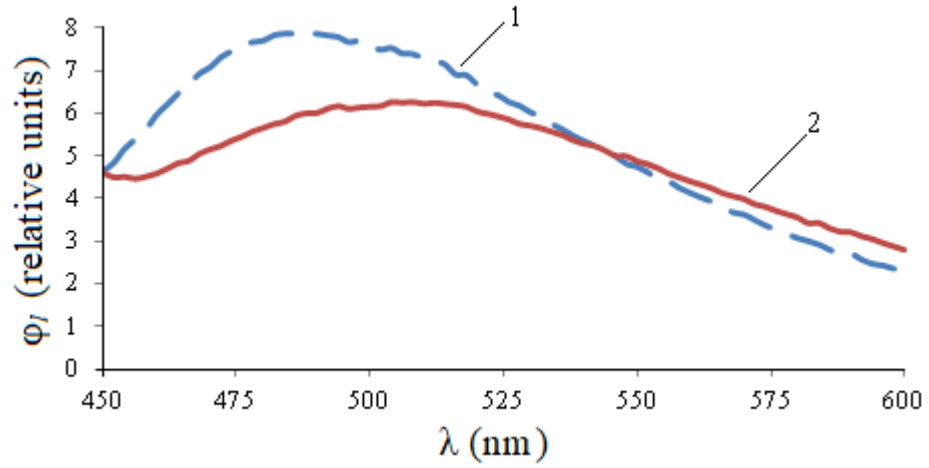

Figure 5. Spectral characteristics of luminescence of wheat seeds at $\lambda_{e,3}$ = 424 nm: 1—not infected, 2—98% infected.

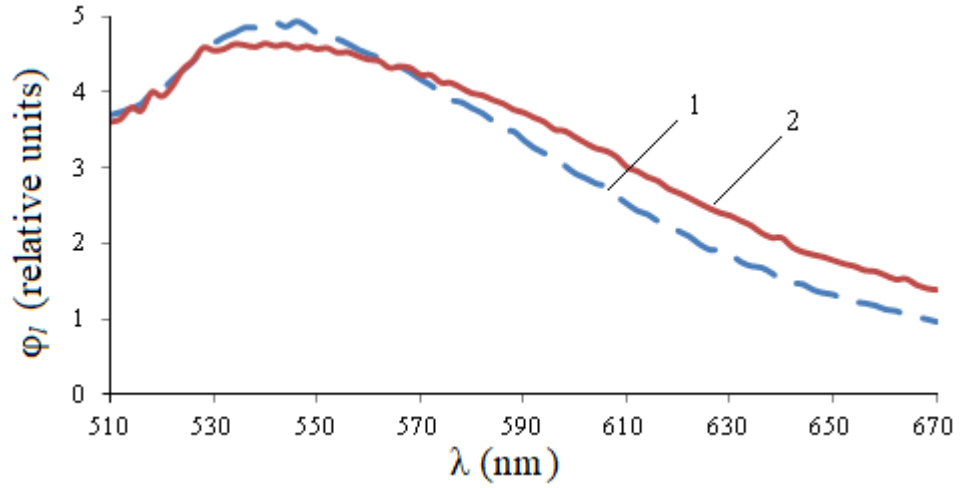

Figure 6. Spectral characteristics of luminescence of wheat seeds at $\lambda_{e,4}$ = 485 nm: 1—not infected, 2—98% infected.

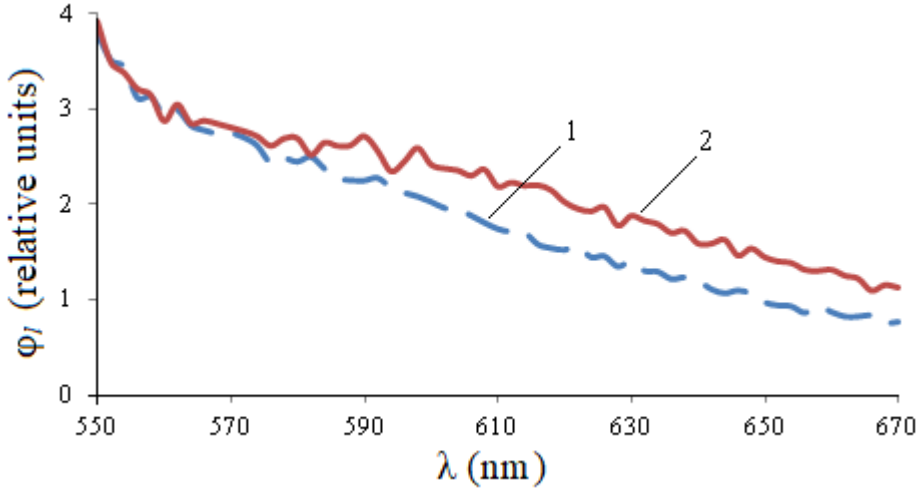

Figure 7. Spectral characteristics of luminescence of wheat seeds at $\lambda_{e/5}$ = 528 nm: 1—not infected, 2—98% infected.

Similar calculations were performed for other wavelengths of the excitation maxima.

The luminescence range at a given excitation wavelength is 390–550 nm (Figure 4). At the same time, also for infected seeds, the relative photoluminescence flux is 1.44 times higher, the maximum value is 1.36 times higher.

In Figure 5, the entire photoluminescence range is 450–600 nm, but in the 450–550 nm area, the curve for healthy seeds is noticeably higher than the curve for infected seeds, and in the 550–600 nm area, quantitative changes are practically indistinguishable. The integral flow of healthy seeds exceeds the flow of infected seeds by 1.12 times, the maximum value is 1.29 times, but the wavelength of the maximum is shifted by 25 nm to the right.

In Figure 6, the photoluminescence spectrum of healthy seeds exceeds the spectrum of infected seeds at a site of 530–560 nm, and then becomes smaller. The integral flow of infected seeds exceeds the flow of healthy seeds by 1.09 times, the maximum value is 1.07 times.

It follows from Figure 7 that there is practically no luminescence at the excitation of λ_e = 528 nm. The rise of the graphs in the left part is explained by the influence of exciting radiation.

It is advisable to analyze the spectra, determining their parameters, with the help of which it is possible to understand the most significant features of the photoluminescence spectra. The following numerical parameters, well-known from mathematical statistics, determined by Formulas (3)–(10), were used for the analysis.

The calculation results are presented in Table 3.

Table 3. Statistical parameters of photoluminescence spectra of wheat seeds.

λ_e, nm	M_λ, nm	σ^2	μ_3	μ_4	A_S	E_λ	E, eV	Φ, r. u.
healthy seeds								
232	341	310	−6869	255,255	−1.26	−0.34	3.83	36
362	465	1001	2463	2.38	0.08	−3.00	2.69	387
424	509	926	11,538	2.13	0.40	−3.00	2.44	833
485	565	746	8486	1.42	0.42	−3.00	2.20	501
infected seeds								
232	330	269	−249	169,071	−0.06	35.32	3.76	95
362	466	1665	12,174	5.78	0.18	−3.00	2.68	556
424	521	865	5492	1.74	0.21	−3.00	2.39	746
485	571	761	12,611	1.51	0.60	−3.00	2.15	545

Table 3 shows that the mathematical expectations of healthy and infected seeds differ more strongly when excited by wavelengths $\lambda_{e,1}$ = 232 nm (on 11 nm), $\lambda_{e,3}$ = 424 nm (on 12 nm) and less important (on 6 nm) at $\lambda_{e,4}$ = 485 nm, and on $\lambda_{e,2}$ = 362 nm do not almost differ. The variance differences are significant only for $\lambda_{e,2}$ = 362 nm. The statistical moment of the third order μ_3 for $\lambda_{e,1}$ = 232 nm is negative and is 27.7 times different for healthy and infected seeds. The statistical moments of μ_3 are positive and differ less significantly by 1.5–4.9 times for remaining excitation wavelengths. The statistical moment of the fourth-order μ_4 at $\lambda_{e,1}$ = 232 nm is very large in absolute value compared to others. The value of the asymmetry A_S behaves similar to a statistical moment of the third order. The value of the kurtosis E_λ differs only at $\lambda_{e,1}$ = 232 nm for infected and healthy seeds. Moreover, the difference can be traced both by the absolute value of 103 times, and by the sign. The difference in the energy of the spectrum for healthy and infected seeds is relatively small (up to 2.3%) for all wavelengths of excitation.

Spectral characteristics of photoluminescence, decomposition into Gaussians, are presented in Figures 8–11.

The greatest interest in the analysis of the spectra of infected and uninfected seeds decomposed into Gaussians is the ratio of the maxima of the decomposition curves 2 and 3 (Figures 8–11). For healthy seeds at $\lambda_{e,1}$ = 232 nm, the ratio between the maxima of the main (central) and right curves for healthy seeds is 3.71 times, and for infected seeds it decreases to 2.88 times, i.e., by 1.29 times. At $\lambda_{e,2}$ = 362 nm, the ratio is 1.38 times for healthy seeds, and 1.12 times for infected ones. For excitation by radiation, the wavelength of 424 nm and 485 nm, there are no changes in the ratios.

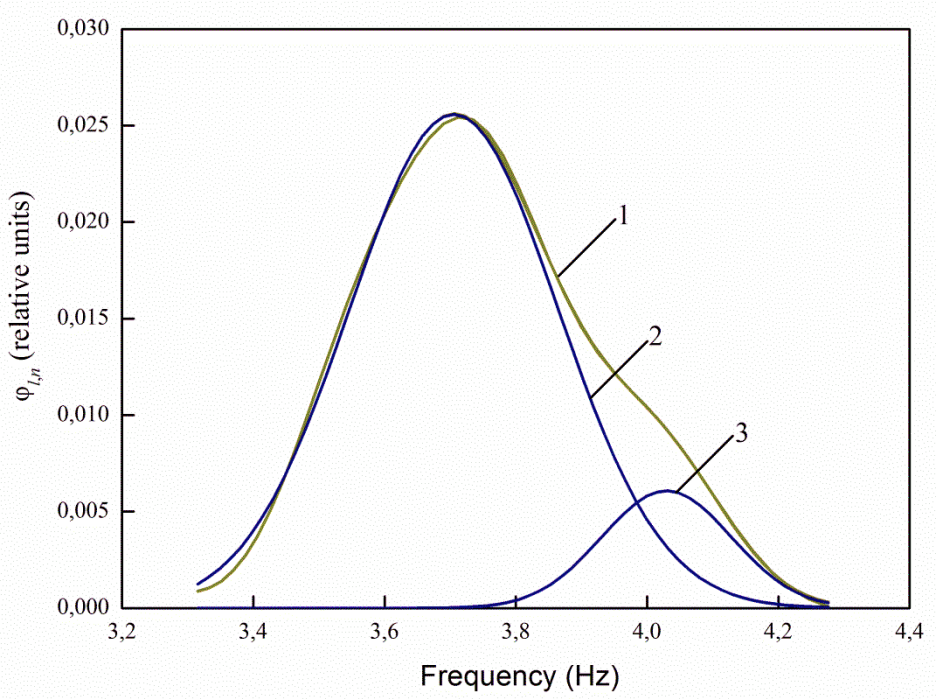

Figure 8. The spectral characteristic of the luminescence of uninfected replacements of wheat at $\lambda_{e,1}$ = 232 nm (1), decomposition by Gaussian curves (2) and (3), where $\varphi_{l,n}$ is the normalized photoluminescence intensity.

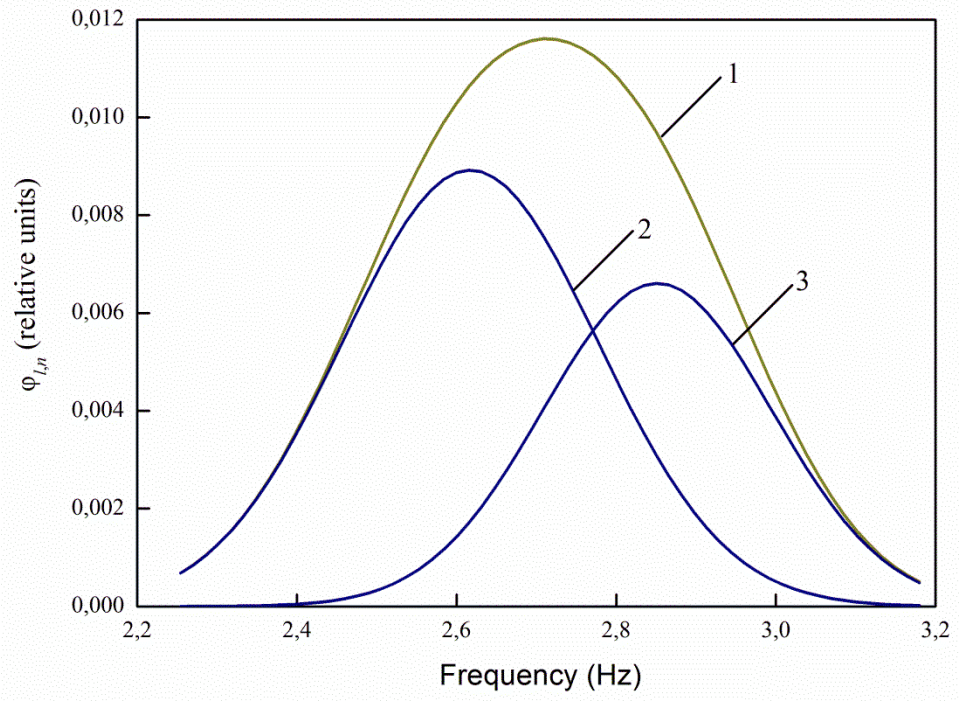

Figure 9. The spectral characteristic of the luminescence of uninfected replacements of wheat at $\lambda_{e,2}$ = 362 nm (1), decomposition by Gaussian curves (2) and (3).

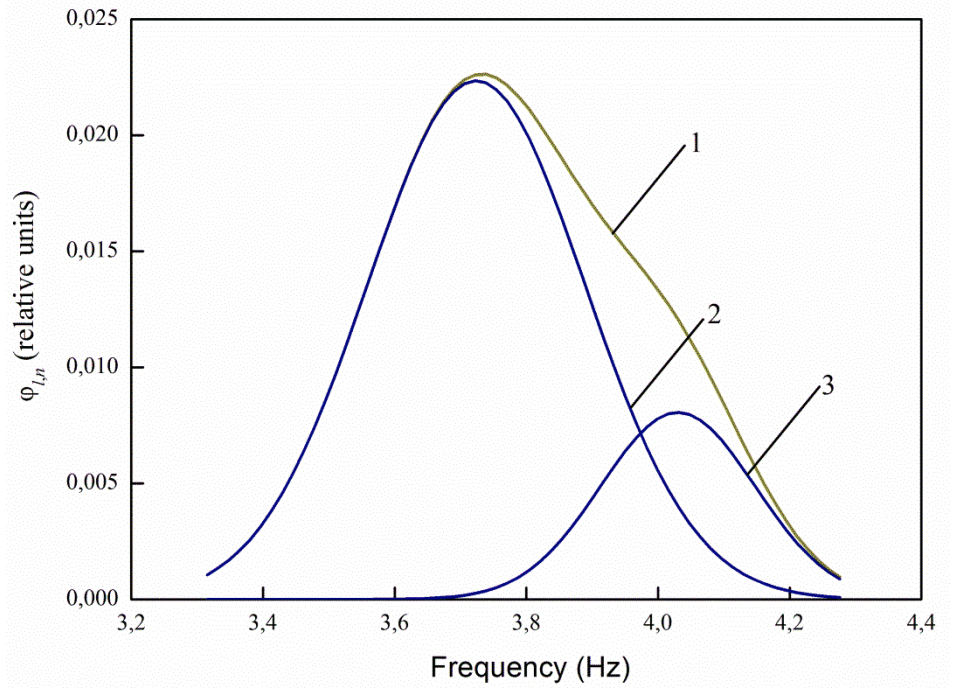

Figure 10. The spectral characteristic of the luminescence of infected wheat changeover at $\lambda_{e,1}$ = 232 nm (1), decomposition by Gaussian curves (2) and (3).

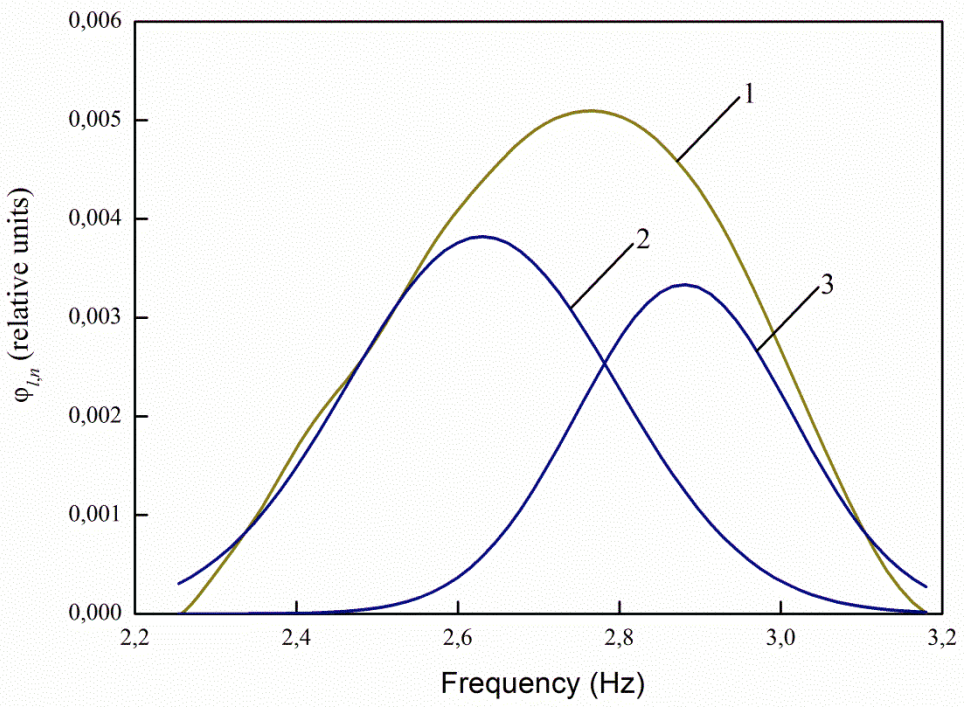

Figure 11. The spectral characteristic of the luminescence of infected wheat replacements at $\lambda_{e,2}$ = 362 nm (1), decomposition by Gaussian curves (2) and (3).

4. Discussion

The most informative spectral range of diagnostics of winter wheat seeds is 220–400 nm. When infected with fusarium, a new excitation maximum appears at a wavelength of 232 nm and a maximum of 362 nm increases, which is practically unnoticeable in healthy ripe seeds. The early appearance of the excitation peak at 362 nm and an increase in the photoluminescence flux from it were observed in immature seeds of cereals (wheat, oats, and corn) [24]. This may indicate a slowdown in the maturation processes of infected seeds. The photoluminescence flux increases significantly (by 1.44–2.64 times) in infected seeds, which can be easily detected by a photodetector. Such differences are significant, since the error in determining the flow does not exceed 2% for reliability of 0.9.

For healthy and infected seeds in the photoluminescence range of 290–374 nm, the mathematical expectation (by 11–12 nm), the statistical moment of the third order (up to 27.7 times), asymmetry (up to 21 times), kurtosis (up to 103 times) change significantly. The ratio between the maxima of individual bands obtained by the decomposition of Gaussian functions decreases by 29% when excited by $\lambda_{e,1}$ = 232 nm and by 23% when excited by $\lambda_{e,2}$ = 362 nm. In other photoluminescence ranges, the difference between the parameters of healthy and infected seeds is either significantly less or non-existent. Thus, the best markers for detecting pathogenic *Fusarium* microflora are the excitation wavelengths of 232 nm and 362 nm.

5. Conclusions

Spectral differences of excitation and photoluminescence of winter wheat seeds in the short-wave range (220–400 nm) during infection were revealed. There are differences in the statistical parameters of the spectra and Gaussians during decomposition. Based on the results obtained on wheat seeds, further development of a methodology for determining the degree of infection with fusarium is possible.

Author Contributions: Conceptualization, A.M.B. and M.V.B.; methodology, M.V.B.; software, I.Y.E. and A.A.G.; validation, A.A.B.; formal analysis, A.V.L.; investigation, I.Y.E., S.A.G. and S.I.B.; resources, A.A.G. and A.A.B.; data curation, M.V.B. and I.Y.E.; writing—original draft preparation, M.V.B.; writing—review and editing, A.M.B.; visualization, I.Y.E.; supervision, A.A.G. and A.V.L.; project administration, M.V.B. and A.A.G.; funding acquisition, M.V.B., S.I.B. and A.A.G. All authors have read and agreed to the published version of the manuscript.

Funding: This work was supported by a grant of the Ministry of Science and Higher Education of the Russian Federation for large scientific projects in priority areas of scientific and technological development (grant number 075-15-2020-774).

Institutional Review Board Statement: Not applicable.

Informed Consent Statement: Not applicable.

Conflicts of Interest: The authors declare no conflict of interest.

References

1. Pu, J.; Xie, Y.; Zhang, H.; Zhang, X.; Qi, Y.; Peng, J. Development of a real-time fluorescence loop-mediated isothermal amplification assay for rapid and quantitative detection of *Fusarium mangiferae* associated with mango malformation. *Physiol. Mol. Plant Pathol.* **2014**, *86*, 81–88. [CrossRef]
2. Edwards, S.G.; O'Callaghan, J.; Dobson, A.D. PCR-based detection and quantification of mycotoxigenic fungi. *Mycol. Res.* **2002**, *106*, 1005–1025. [CrossRef]
3. Priyadarshini, P.; Kohli, D.; Yadav, S.; Srinivasa, N.; Bharadwaj, C.; Anjoy, P.; Gaikwad, K.; Jain, P.K. Quantitative detection of pathogen load of *Fusarium oxysporum* f.sp. ciceris infected wilt resistant and susceptible genotypes of chickpea using intergenic spacer region-based marker. *Physiol. Mol. Plant Pathol.* **2021**, *114*, 101622. [CrossRef]
4. Barbedo, J.G.; Guarienti, E.M.; Tibola, C.S. Detection of sprout damage in wheat kernels using NIR hyperspectral imaging. *Biosyst. Eng.* **2018**, *175*, 124–132. [CrossRef]
5. Liang, P.-S.; Haff, R.P.; Hua, S.-S.T.; Munyaneza, J.E.; Mustafa, T.; Sarreal, S.B.L. Nondestructive detection of zebra chip disease in potatoes using near-infrared spectroscopy. *Biosyst. Eng.* **2018**, *166*, 161–169. [CrossRef]
6. Moomkesh, S.; Mireei, S.A.; Sadeghi, M.; Nazeri, M. Early detection of freezing damage in sweet lemons using Vis/SWNIR spectroscopy. *Biosyst. Eng.* **2017**, *164*, 157–170. [CrossRef]
7. Ibrahim, A.; Csúr-Varga, A.; Jolánkai, M.; Mansour, H.; Hamed, A. Monitoring some quality attributes of different wheat varieties by infrared technology. *Agric. Eng. Int. CIGR J.* **2018**, *20*, 201–210.
8. Liu, C.; Pinto, F.; Cossani, C.M.; Sukumaran, S.; Reynolds, M.P. Spectral reflectance indices as proxies for yield potential and heat stress tolerance in spring wheat: Heritability estimates and marker-trait associations. *Front. Agric. Sci. Eng.* **2019**, *6*, 296. [CrossRef]
9. Lee, H.; Kim, M.S.; Lim, H.-S.; Park, E.; Lee, W.-H.; Cho, B.-K. Detection of cucumber green mottle mosaic virus-infected watermelon seeds using a near-infrared (NIR) hyperspectral imaging system: Application to seeds of the "Sambok Honey" cultivar. *Biosyst. Eng.* **2016**, *148*, 138–147. [CrossRef]
10. Whetton, R.L.; Hassall, K.L.; Waine, T.W.; Mouazen, A.M. Hyperspectral measurements of yellow rust and fusarium head blight in cereal crops: Part 1: Laboratory study. *Biosyst. Eng.* **2018**, *166*, 101–115. [CrossRef]
11. Bock, C.H.; Barbedo, J.G.A.; Del Ponte, E.M.; Bohnenkamp, D.; Mahlein, A.-K. From visual estimates to fully automated sensor-based measurements of plant disease severity: Status and challenges for improving accuracy. *Phytopathol. Res.* **2020**, *2*, 9. [CrossRef]
12. Barbedo, J.G.A. A review on the main challenges in automatic plant disease identification based on visible range images. *Biosyst. Eng.* **2016**, *144*, 52–60. [CrossRef]
13. Mahlein, A.-K.; Kuska, M.T.; Behmann, J.; Polder, G.; Walter, A. Hyperspectral sensors and imaging technologies in phytopathology: State of the art. *Annu. Rev. Phytopathol.* **2018**, *56*, 535–558. [CrossRef]
14. Brugger, A.; Behmann, J.; Paulus, S.; Luigs, H.-G.; Kuska, M.T.; Schramowski, P.; Kersting, K.; Steiner, U.; Mahlein, A.-K. Extending Hyperspectral Imaging for Plant Phenotyping to the UV-Range. *Remote Sens.* **2019**, *11*, 1401. [CrossRef]
15. Wahabzada, M.; Mahlein, A.-K.; Bauckhage, C.; Steiner, U.; Oerke, E.-C.; Kersting, K. Metro Maps of Plant Disease Dynamics—Automated Mining of Differences Using Hyperspectral Images. *PLoS ONE* **2015**, *10*, e0116902. [CrossRef]
16. Thomas, S.; Kuska, M.T.; Bohnenkamp, D.; Brugger, A.; Alisaac, E.; Wahabzada, M.; Behmann, J.; Mahlein, A.-K. Benefits of hyperspectral imaging for plant disease detection and plant protection: A technical perspective. *J. Plant Dis. Prot.* **2018**, *125*, 5–20. [CrossRef]
17. Noh, H.K.; Lu, R. Hyperspectral laser-induced fluorescence imaging for assessing apple fruit quality. *Postharvest Biol. Technol.* **2007**, *43*, 193–201. [CrossRef]
18. Saleem, M.; Atta, B.M.; Ali, Z.; Bilal, M. Laser-induced fluorescence spectroscopy for early disease detection in grapefruit plants. *Photochem. Photobiol. Sci.* **2020**, *19*, 713–721. [CrossRef] [PubMed]

19. Belasque, J.J.; Gasparoto, M.C.G.; Marcassa, L.G. Detection of mechanical and disease stresses in citrus plants by fluorescence spectroscopy. *Appl. Opt.* **2008**, *47*, 1922–1926. [CrossRef]
20. Sarimov, R.M.; Lednev, V.N.; Sibirev, A.V.; Gudkov, S.V. The Use of Fluorescence Spectra for the Detection of Scab and Rot in Fruit and Vegetable Crops. *Front. Phys.* **2021**, *8*, 640887. [CrossRef]
21. Belyakov, M.V.; Kulikova, M.G. Control of bulk products' humidity and grinding size by the photoluminescent method photoluminescent quality control. *J. Food Process. Preserv.* **2020**, *44*, e14640. [CrossRef]
22. Kovalenko, A.V.; Vovk, S.M.; Plakhtii, Y.G. Sum Decomposition Method for Gaussian Functions Comprising an Experimental Photoluminescence Spectrum. *J. Appl. Spectrosc.* **2021**, *88*, 357–362. [CrossRef]
23. Zienko, S.; Belyakov, M.; Malyschkin, V. Investigation of luminescence spectra of the plant tissue cover tissue. *Appl. Phys.* **2018**, *3*, 43–48. (In Russian)
24. Belyakov, M.; Sokolova, E.; Listratenkova, V.; Ruzanova, N.; Kashko, L. Photoluminescent Control Ripeness of the Seeds of Plants. *E3S Web Conf.* **2021**, *273*, 1003. [CrossRef]